RAA 2016 Vol. **16** No. **5**, 82 (8pp) doi: 10.1088/1674–4527/16/5/082
http://www.raa-journal.org *http://iopscience.iop.org/raa*

***R**esearch in*
***A**stronomy and*
***A**strophysics*

Diagnosing physical conditions near the flare energy-release sites from observations of solar microwave type III bursts

Bao-Lin Tan[1], Marian Karlický[2], Hana Mészárosová[2] and Guang-Li Huang[3]

[1] Key Laboratory of Solar Activity, National Astronomical Observatories, Chinese Academy of Sciences, Beijing 100012, China; *bltan@nao.cas.cn*
[2] Astronomical Institute of the Academy of Sciences of the Czech Republic, CZ–25165 Ondřejov, Czech Republic
[3] Purple Mountain Observatory, Chinese Academy of Sciences, Nanjing 210008, China

Received 2015 October 10; accepted 2015 November 24

Abstract In the physics of solar flares, it is crucial to diagnose the physical conditions near the flare energy-release sites. However, so far it is unclear how to diagnose these physical conditions. A solar microwave type III burst is believed to be a sensitive signature of primary energy release and electron accelerations in solar flares. This work takes into account the effect of the magnetic field on the plasma density and develops a set of formulas which can be used to estimate the plasma density, temperature, magnetic field near the magnetic reconnection site and particle acceleration region, and the velocity and energy of electron beams. We apply these formulas to three groups of microwave type III pairs in an X-class flare, and obtained some reasonable and interesting results. This method can be applied to other microwave type III bursts to diagnose the physical conditions of source regions, and provide some basic information to understand the intrinsic nature and fundamental processes occurring near the flare energy-release sites.

Key words: Sun: radio radiation — Sun: flares — Sun: corona

1 INTRODUCTION

In solar flares, energetic particles play a prominent role in energy release, transmission, conversion and emission propagation. Estimation shows that energetic particles may carry about 10%–50% of the total energy released in a typical X-class flare (Lin & Hudson 1976). However, so far, there are many unresolved problems related to solar energetic particles, especially energetic electrons, such as where is the site of electron acceleration? What is the exact mechanism of particle acceleration? How fast are the energetic electron beams flying away from their source region? It is necessary to accurately measure the physical conditions around the source region for answering the above questions. These conditions include plasma density, temperature, magnetic field and energy of particle beams (Zharkova et al. 2011).

A solar radio type III burst is believed to be a sensitive signature of the energetic electron beams that are generated and which propagate in the corona. It is interpreted as being caused by an energetic electron beam streaming through the background plasma at a speed of about 0.1–0.9 c (c is the speed of light) propagating away from the acceleration site (e.g., Lin & Hudson 1971; Lin et al. 1981; Huang et al. 2007 and a recent review in Reid & Ratcliffe 2014). In meter or longer wavelengths, solar radio type III bursts are regarded as being generated by energetic electron beams propagating upward in open magnetic field configurations. Their frequency drift rates are negative and are called normal type III bursts and their emission source may be located above the flare energy-release site. But in decimeter- or shorter wavelengths, the frequency drift rates of type III bursts are always positive. We call them microwave type III bursts which are believed to be produced by the electron beams propagating downward. Their emission source may be located below the flare energy-release site. Occasionally there will be simultaneously observed microwave type III burst pairs, which are composed of normal type III branches with negative frequency drift rates and reversed slope (RS) type III branches with positive frequency drift rates. Microwave type III pairs are explained as being produced by bi-directional electron beams and their source regions are very close to the flare energy-release site where the magnetic reconnection and particle acceleration take place. Therefore, microwave type III bursts, including the microwave type III pairs, are the most important tool for diagnosing the physical conditions around the flare energy-release sites. They may provide the most important information for understanding the flare triggering mechanism and particle acceleration.

The short lifetimes and very high brightness temperatures of microwave type III bursts indicate that the emis-

sion should be a coherent process. The first coherent mechanism is electron cyclotron maser emission (Melrose & Dulk 1982; Tang et al. 2012) which requires a strong background magnetic field such that $f_{\rm ce} > f_{\rm pe}$. $f_{\rm ce}$ is electron gyro-frequency and $f_{\rm pe}$ is plasma frequency. As for microwave type III bursts, the required magnetic fields should be $B > 1000\,{\rm G}$, too strong to occur in the solar corona. The second coherent mechanism is plasma emission (PE, Zheleznyakov & Zlotnik 1975) which is generated from the coupling of two excited plasma waves at a frequency of $2f_{\rm pe}$ (second harmonic PE), or the coupling of an excited plasma wave and a low-frequency electrostatic wave at a frequency of about $f_{\rm pe}$ (fundamental PE). As PE has no strong magnetic field constraints, it is the favored mechanism for type III bursts.

In the PE mechanism, the emission frequency can be expressed as

$$f \approx 9sn_{\rm e}^{\frac{1}{2}}. \tag{1}$$

The units of f and $n_{\rm e}$ are Hz and $\rm m\,s^{-3}$, respectively. s is the harmonic number, and $s = 1$ is the fundamental PE while $s = 2$ is the second harmonic PE. Generally, the fundamental PE has strong circular polarization while the second harmonic PE always has relatively weak circular polarization.

The frequency drift rate is the most prominent observed parameter of microwave type III bursts, which is connected to many physical conditions in the source region. From Equation (1), we derive

$$\begin{aligned} D = \frac{df}{dt} &= \frac{f}{2}\left(\frac{\partial n_{\rm e}}{n_{\rm e}\partial t} + \frac{\partial n_{\rm e}}{n_{\rm e}\partial l}\cdot\frac{\partial l}{\partial t}\right) \\ &= \frac{f}{2}\left(\frac{1}{t_n} + \frac{v_b}{H_n}\right). \end{aligned} \tag{2}$$

The relative frequency drift rate is expressed as

$$\bar{D} = \frac{df}{fdt} = \frac{1}{2t_n} + \frac{v_b}{2H_n}. \tag{3}$$

$H_n = \frac{n_{\rm e}}{\partial n_{\rm e}/\partial l}$ is the plasma density scale length along the electron beams. $H_n > 0$ or $H_n < 0$ means the density is increasing or decreasing respectively along the electron beam. $t_n = \frac{n_{\rm e}}{\partial n_{\rm e}/\partial t}$ is the plasma density time scale. $t_n > 0$ or $t_n < 0$ means the density is increasing or decreasing with respect to time. $\frac{\partial l}{\partial t} = v_b$ is the velocity of electron beams.

Equations (2) and (3) show that frequency drift rate is composed of two parts. The first part is related to the temporal variation of plasma density, and the second part is related to the spatial variation of plasma density which is caused by a plasma density gradient and the motion of electron beams.

In the flare impulsive phase, fast magnetic reconnection may produce plasma inflows into the reconnecting region and result in plasma density increasing, $t_n > 0$. In the post-flare phase, magnetic reconnection becomes very weak, and there is no obvious variation of the plasma density, $t_n \to \infty$ and the first term of Equations (2) and (3) can be neglected.

H_n depends on plasma density distributions (Dulk 1985). So far, the most common plasma density models of the quiet solar atmosphere are the Baumbach-Allen model (Allen 1947) and Newkirk model (Newkirk 1967). When applying these models to an active region, it is always necessary to multiply by a factor from 3 to 50. Naturally, this method has a large uncertainty. By using the broadband radio spectral observations of the solar eclipse, Tan et al. (2009) obtained an improved semi-empirical model of the coronal plasma density. However, the above models are expressed as functions of height from the solar surface. It is difficult to apply them to a microwave type III burst at a certain frequency when the height of the source region is not known. Under the assumption of a static and barometric solar atmosphere, H_n can be estimated as $H_n = -\frac{k_{\rm B}T}{m_0 g}$ (Benz et al. 1983). $k_{\rm B}$ is the Boltzmann constant, g the solar gravitational acceleration ($\sim$274 $\rm m\,s^{-2}$ near the solar surface), and m_0 the average mass of ions in the solar chromosphere and corona. The minus sign indicates the density is decreasing with respect to height. The barometric model is only valid in the quiet corona and is not appropriate for the type III-emitting source region that cannot be in hydrodynamic equilibrium because of substantial heating and plasma flows. The generated microwaves are subject to free-free absorption when they propagate in the ambient plasma, and they will be strongly absorbed. Assuming the plasma is isothermal and barometric, then the density length scale corresponding to the optical depth of unity is about $H_n \approx 6.67\times10^{14}\frac{T^{3/2}}{f^2}$ (m) for the fundamental emission and $H_n \approx 1.07\times10^{16}\frac{T^{3/2}}{f^2}$ (m) for the harmonic emission (Dulk 1985, Stahli & Benz 1987). But when applying this expression to estimate the electron beam velocity, we find $v_b > 1.0\,c$ in some events, and $v_b < 0.1\,c$ in other events. These results are unreasonable. Aschwanden et al. (1995) proposed a combined model by assuming a power-law function in the lower corona and an exponential function in the upper corona. However, as the above models have not considered the effect of magnetic fields, they cannot reflect the relationship between the physical conditions and properties of the microwave type III bursts.

This work proposes a new method for diagnosing the physical conditions around the flaring energy-release sites from observations of solar microwave type III bursts. Section 2 introduces the main observable parameters of microwave type III bursts. In Section 3, we derive a new expression for the plasma density length scale (H_n) from the full MHD equation which contains magnetic pressure force. On this basis, we proposed a set of formulas to estimate the plasma density, temperature, magnetic field around the primary source region of solar flares, and the velocity and energy of the energetic electron beams. In Section 4, we apply the above method to diagnose the source region of three groups of microwave type III burst

pairs in the post-flare phase of an X-class flare. Finally, conclusions are summarized in Section 5.

2 OBSERVING PARAMETERS OF MICROWAVE TYPE III BURSTS

Recently, there have been many solar radio spectrometers that have been operating at a frequency in the microwave range with high frequency and time resolutions. For example, the Chinese Solar Broadband Radio Spectrometer (SBRS) at Huairou Observing Station operates with dual circular polarization (left- and right-handed circular polarizations) in the frequency range of 1.10–2.06 GHz, 2.60–3.80 GHz and 5.20–7.60 GHz. The cadence is 5–8 ms and the frequency resolution is 4–20 MHz (Fu et al. 1995, 2004, Yan et al. 2002). The Ondřejov radiospectrograph in the Czech Republic operates in a frequency range of 0.80–5.00 GHz. Its cadence is 10 ms and the frequency resolution is 5–12 MHz (Jiricka et al. 1993).

From the observations of microwave type III bursts, we can derive several observable parameters:

(1) Start frequency ($f_{\rm st}$), defined as the frequency at the starting point of the microwave type III burst with emission intensity significantly exceeding the background.
(2) Burst lifetime (τ), defined as the time difference between the start and end of an individual type III burst.
(3) Central frequency (f_0), defined as the frequency at the midpoint of a type III burst.
(4) Frequency drift rate ($D = \frac{df}{dt}$), defined as the slope of a type III burst on a spectrogram. f is the frequency at the ridge crest along the type III burst at different times. Generally, frequency drift rate can be derived by using cross-correlation analysis at each of two adjacent frequency channels.
(5) The relative frequency drift rate ($\bar{D}$), defined as $\bar{D} = \frac{df}{fdt} \approx \frac{D}{f_0}$.

3 DIAGNOSTICS OF THE FLARE ENERGY-RELEASE SITE

In order to understand the process of microwave type III bursts, we construct a physical scenario to roughly demonstrate the possible processes of magnetic reconnection, and particle accelerations and propagations associated with microwave type III bursts in solar flares (Fig. 1). Here magnetic reconnection may take place in a cusp configuration above and very close to the top of the flaring loop similar to a Masuda-like flare (Masuda et al. 1994, etc.), or in the current sheet above and beyond flare loops triggered by the tearing-mode instability (Kliem et al. 2000, etc.). In some flares the reconnections are more dominated by cusp configuration and in other flares they are dominated by current sheets. Electrons are accelerated in the reconnection site (source region), propagate upward or downward, and produce normal or RS type III bursts.

In this section, a new diagnostic method can be derived in the framework of the above physical scenarios.

3.1 Constraints on the Emission Process

As we mentioned in Section 1, the most probable emission mechanism of microwave type III bursts is the PE. There are some constraints on this mechanism for certain microwave type III bursts (Cairns & Melrose 1985, Robinson & Benz 2000):

(1) Magnetic field. $f_{\rm ce} < f_{\rm pe}$ and $f > f_{\rm pe}$ require a relatively weak magnetic field of $B < 3.57 \times 10^{-7} f$ (G). Here, the unit of f is Hz. For example, the magnetic field must be $B < 1070\,{\rm G}$ at a frequency of 3 GHz. For most cases, this condition is easy to satisfy.
(2) Emission Frequency. PE mechanism is a three-wave interaction process, which must satisfy the frequency condition $f_{\rm T} = f_{\rm L} + f_3$. Here subscripts T, L and 3 represent the transverse radiation, Langmuir wave and third wave, respectively. When the third wave is an ion-sound wave, it will produce fundamental emission; and a second harmonic emission will be produced when the third wave is a secondary Langmuir wave.
(3) Beam direction. The three-wave interaction requires wave-vector conservation $k_{\rm T} = k_{\rm L} + k_3$. Here, $k_{\rm L}$ is almost in the direction of the electron beams, but values for k_3 have broad distributions. As for the fundamental emission, k_3 represents an ion-sound wave and for $k_3 \ll k_{\rm L}$ the emission ($k_{\rm T}$) is approximately in the same direction as the electron beams. As for the second harmonic emission, k_3 represents a secondary Langmuir wave and $k_{\rm T}$ may obviously deviate from the electron beams.
(4) Beam velocity. Not all electron beams can generate Langmuir waves to produce a certain type III burst; actually only a beam with a positive derivative in its distribution function in velocity space can produce Langmuir waves by bump-in-tail instability. The positive derivative in its distribution function must be formed on the total distribution function (background Maxwellian distribution + beam distribution), and this means that the velocity of the electron beam must exceed a lower limit which is above the thermal velocity of the background Maxwellian distribution, especially for low density beams

$$v_b > 3.2 \times 10^2 (n_{\rm e}\tau)^{1/3} = v_{\rm L}\,. \quad (4)$$

The above equation is derived from the relationship $\tau < t_{\rm d}$. τ is the observed lifetime of a microwave type III burst. $t_{\rm d} = 3.1 \times 10^{-8} \frac{v_b^3}{n_{\rm e}}$ is the collisional deflection time of the electron beams, where the units of $v_{\rm b}$ and $n_{\rm e}$ are m s^{-1} and m^{-3}, respectively (Benz et al. 1992). The lower limit indicates that a low energy electron beam will be dissipated in dense plasma and cannot produce coherent emission.

At the same time, the dispersion relation of PE emission also requires an upper velocity limit of

$$v_b < \frac{3}{2}\sqrt{\frac{m_{\rm i}}{\gamma m_{\rm e}}} V_0 = v_H\,. \quad (5)$$

Here $\gamma = 1 + 3\frac{T_\mathrm{i}}{T_\mathrm{e}} \approx 2$, V_0 is the electron thermal velocity, v_H is a critical velocity ($\approx 40 - 50V_0$), m_e and m_i are electron and mean ion mass, and T_i and T_e are ion and electron temperatures, respectively. The upper velocity limit indicates that a very high energy electron beam will not produce PE when propagating in cold plasmas. In very hot plasma, for example, when $T_\mathrm{e} \approx 3\times10^6$ K, $v_H \approx c$. In such a case, the upper limit is the speed of light. The full velocity constraint for a PE-emitting electron beam is $v_\mathrm{L} < v_b < v_H$. This constraint is very meaningful for estimating the magnetic field near source regions. We will demonstrate it in Section 3.5.

3.2 Plasma Density and Temperature

The emission of a microwave type III burst is generated close to the flare primary source region. By using the observed start frequency (f_st), the plasma density near the start site of the electron beam can be obtained from Equation (1)

$$n_\mathrm{st} = f_\mathrm{st}^2/81s^2\ (\mathrm{m}^{-3}). \tag{6}$$

The temperature can be derived approximately from the ratio of soft X-ray (SXR) intensities at two energy bands observed by the GOES satellite after subtracting the background by using Solar Software (Thomas et al. 1985). Applying this method, we obtain the temperature profiles in each flare. From these profiles, we can get the temperature at the time of the microwave type III burst. However, it is important to note that the above temperature is only related to the hot flaring loops which are possibly different from the real source region of microwave type III bursts.

3.3 Frequency Drift Rates

Equations (2) and (3) indicate that the frequency drift rate of a microwave type III burst is composed of two parts. When the temporal change is neglected, the frequency drift rate only depends on the ratio between the beam velocity (v_b) and the density scale length (H_n) along the path of the source (Benz et al. 1983). Therefore, H_n is a key factor to estimate the beam velocity from the frequency drift rate of microwave type III bursts. However, as we mentioned in Section 1, there is considerable uncertainty when determining the value of H_n by using the existing methods. None of the above methods have considered the effect of magnetic fields on the plasma density or its distribution.

Actually, magnetic field is a key factor in flare energy-release sites, which compresses and confines plasma, and dominates the plasma density and its distribution. As a consequence, H_n is also dominated by the magnetic field. In this section, we try to deduce an expression for H_n from a full MHD equation including plasma thermal pressure force (∇p), Lorentz force ($\boldsymbol{j} \times \boldsymbol{B}$) and gravitational force ($\rho \boldsymbol{g}$),

$$\frac{d(\rho \boldsymbol{v})}{dt} = -\nabla p + \boldsymbol{j} \times \boldsymbol{B} + \rho \boldsymbol{g}\,. \tag{7}$$

In quasi-equilibrium, $\frac{d(\rho \boldsymbol{v})}{dt} \sim 0$, $\nabla p \sim \frac{n_\mathrm{e} k_\mathrm{B} T}{H_n}$. The Lorentz force can be decomposed into

$$\boldsymbol{j} \times \boldsymbol{B} = \frac{1}{\mu_0}\Big(\boldsymbol{B}\cdot\nabla\Big)\boldsymbol{B} - \nabla\Big(\frac{B^2}{2\mu_0}\Big)\,. \tag{8}$$

Furthermore, the first and second terms on the right side can be expressed respectively as,

$$\frac{1}{\mu_0}\Big(\boldsymbol{B}\cdot\nabla\Big)\boldsymbol{B} = \frac{d}{ds}\Big(\frac{B^2}{2\mu_0}\Big)\boldsymbol{s} + \frac{B^2}{\mu_0 R_\mathrm{c}}\boldsymbol{s} \tag{9}$$

$$-\nabla\Big(\frac{B^2}{2\mu_0}\Big) = -\frac{d}{ds}\Big(\frac{B^2}{2\mu_0}\Big)\boldsymbol{s} - \nabla_\perp\Big(\frac{B^2}{2\mu_0}\Big)\boldsymbol{n}. \tag{10}$$

Here, the unit vector $\boldsymbol{s}$ is along the magnetic field lines, $\boldsymbol{n}$ is normal to the magnetic field lines and R_c is the curvature radius of the magnetic field lines.

Then, substituting Equations (9) and (10) into (8), we have

$$\boldsymbol{j} \times \boldsymbol{B} = \frac{B^2}{\mu_0 R_\mathrm{c}}\boldsymbol{s} - \nabla_\perp\Big(\frac{B^2}{2\mu_0}\Big)\boldsymbol{n}. \tag{11}$$

The first term in Equation (11) is the magnetic tension force which is acting along the direction of the magnetic field, and has a resultant effect only when a magnetic field line is curved. The second term is the magnetic pressure force which is acting in the direction perpendicular to the magnetic field lines, and this force will compress and confine the plasmas (Priest 2014). Any changes in the magnetic field strength will lead to a corresponding variation in plasma density. Therefore, plasma density is dominated by the magnetic field. In the actual condition near the flare energy-release site, there is also a magnetic gradient between different points along the magnetic field lines, and this will lead to a density gradient between the different points along the magnetic field. Substituting Equation (11) into Equation (7), we have,

$$\begin{aligned}\frac{d(\rho \boldsymbol{v})}{dt} \;=\; &-\Big[\nabla_\parallel P - \frac{B^2}{\mu_0 R_\mathrm{c}} + m_0 n_\mathrm{st} g\cos\theta\Big]\boldsymbol{s} \\ &-\Big[\nabla_\perp P + \nabla_\perp\Big(\frac{B^2}{2\mu_0}\Big) - m_0 n_\mathrm{st} g\sin\theta\Big]\boldsymbol{n}.\end{aligned} \tag{12}$$

Here, the plasma thermal pressure $P = n_\mathrm{st} k_\mathrm{B} T_\mathrm{e}$.

Figure 1 indicates that the electron beams are mainly propagating along the magnetic field lines, so we may let the longitudinal component approach zero, $\nabla_\parallel (n_\mathrm{st} k_\mathrm{B} T_\mathrm{e}) \approx \frac{n_\mathrm{st} k_\mathrm{B} T_\mathrm{e}}{H_n}$. H_n is the plasma density scale length along the magnetic field lines,

$$H_n = \frac{k_\mathrm{B} T}{\frac{B^2}{n_\mathrm{st}\mu_0 R_\mathrm{c}} - m_0 g\cos\theta}. \tag{13}$$

Using a barometric atmosphere model with $\boldsymbol{j} \times \boldsymbol{B} \to 0$, we can derive the barometric density scale length $H_n = -\frac{k_\mathrm{B} T}{m_0 g}$ directly from Equation (7). Actually, when the magnetic field is very weak, $B \to 0$, or in a homogeneous magnetic field where $R_\mathrm{c} \to \infty$, the first term in the denominator vanishes, and assuming $\theta \to 0$, Equation (13)

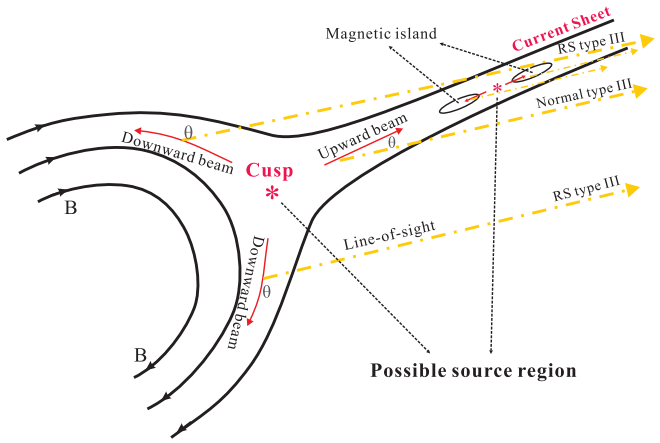

Fig. 1 Schematic diagram illustrating the formation of radio type III burst pairs. Gray solid arrows indicate the path of the energetic electron beams and gray dash-dotted arrows indicate the emission propagation direction.

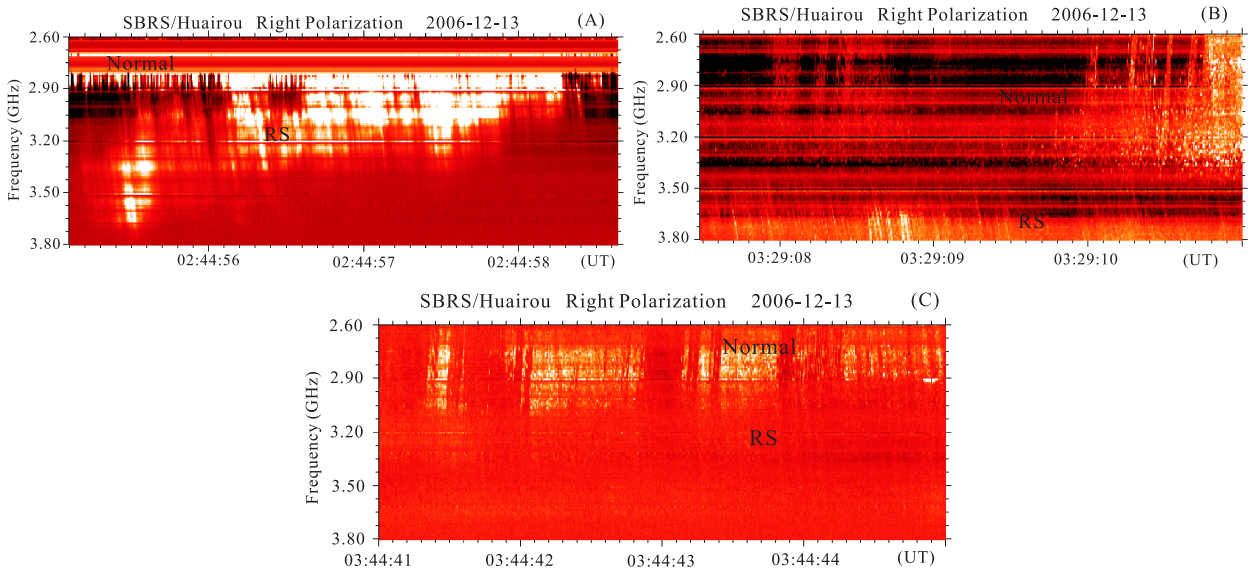

Fig. 2 Three groups of microwave type III pairs at 02:44:56 UT (A), 03:29:09 UT (B) and 03:44:43 UT (C) in the post-flare phase of an X3.4 flare observed at SBRS/Huairou on 2006 December 13.

will degenerate to the barometric form. For example, the radio type III burst at meter or longer wavelengths is generally explained as the propagation of the electron beam in the open magnetic field in the upper corona where the magnetic field is very weak and the curvature radius of the magnetic field lines is much longer. In this case, the barometric model can explain the main properties of radio type III bursts very well.

As for the microwave type III burst, its source region is very close to the acceleration regions and very low. Here the magnetic field is relatively strong, for example, with possible typical values of parameters $B = 20$ G, $n_{\rm st} = 10^{10}$ cm^{-3} and $R_{\rm c} = 10^4$ km, so $\frac{B^2}{n_x \mu_0 R_{\rm c}} \sim 100\ m_0 g$; that means it is very easy to satisfy the relation $\frac{B^2}{n_{\rm st}\mu_0 R_{\rm c}} \gg m_0 g$. This fact implies that the magnetic field does play a dominant role to the plasma density scale length near acceleration regions. Then, Equation (13) can be approximated as

$$H_n \approx \frac{\mu_0 n_{\rm st} k_{\rm B} T}{B^2} R_{\rm c} = \frac{1}{2}\beta_{\rm p} \cdot R_{\rm c}\,. \tag{14}$$

$\beta_{\rm p} = \frac{n_{\rm st} k_{\rm B} T}{B^2/(2\mu_0)}$ is the plasma beta defined as the ratio between the plasma thermal pressure and the magnetic pressure. Equation (14) indicates that the plasma density scale length (H_n) can be replaced by measuring the configuration of the magnetic field ($R_{\rm c}$).

3.4 Electron Beams

Electron beams associated with microwave type III bursts carry important information about the source region, acceleration mechanism, and the trigger mechanism of so-

lar flares. Here, the beam velocity (v_b) is a key parameter that reflects and can derive these properties. From Equations (3) and (14), the beam velocity can be derived,

$$v_b = \frac{\mu_0 n_{\rm st} k_{\rm B} T}{B^2}(2\bar{D} - t_n^{-1})R_{\rm c}\,. \quad (15)$$

The plasma density scale time (t_n) can be derived from the drift rate of the start frequency ($df_{\rm st}/dt$): $t_n = (2\frac{df_{\rm st}}{f_{\rm st}dt})^{-1}$. Observations show that the maximum drift rate of the start frequency is only several MHz per second, and the relative drift rate is $\frac{df_x}{f_x dt} \sim 10^{-3}$ s^{-1}, $t_n^{-1} \sim 10^{-3}$ s^{-1}. The observation shows that the value of $\bar{D}$ ranges from 0.3 s^{-1} to 5.3 s^{-1}. Therefore, we have $\bar{D} \gg t_n^{-1}$, and the term representing plasma density time scale can be neglected. Equation (15) can be approximated as

$$v_b \approx \frac{2\mu_0 n_{\rm st} k_{\rm B} T}{B^2}\bar{D}R_{\rm c}\,. \quad (16)$$

Here, the magnetic field B is not known. Section 3.5 will discuss the method of estimating the magnetic field. The electron beam energy is $E_b \approx 256\frac{\beta^2}{\sqrt{1-\beta^2}}$ (keV). Here, $\beta = v_b/c$.

3.5 Estimation of the Magnetic Field

As mentioned in Section 3.1, there are velocity constraints for PE-emitting electron beams. With these constraints and Equations (15) and (16), an estimation of the magnetic field in the source regions can be derived. The GOES SXR observations show that the temperature near the source regions exceeds 10^7 K and the upper velocity limit is $v_b < c$ (Eq. (5)). Then the lower limit of magnetic fields can be obtained,

$$B_{\rm L} > 3.402 \times 10^{-19}\,\left(n_{\rm st} T|\bar{D}R_{\rm c}|\right)^{1/2}. \quad (17)$$

From the lower limit of beam velocity (Eq. (4)), an upper limit of the magnetic field can be obtained,

$$B_H < 3.293 \times 10^{-16}\,\left[\frac{n_{\rm st} T|\bar{D}R_{\rm c}|}{(n_{\rm st}\tau)^{1/3}}\right]^{1/2}. \quad (18)$$

The unit of magnetic field strength (B) is Tesla. Then the magnetic field near the acceleration region should be in the range of $B_{\rm L} < B < B_H$. The median of the four values should be the best estimator of the real magnetic field strength $B \sim \frac{1}{2}(B_{\rm L} + B_H)$, and the difference between $B_{\rm L}$ and B_H can be regarded as the error limit.

The magnetic field curvature radius $R_{\rm c}$ can be obtained from imaging observations. By using Equations (17) and (18), we may obtain the magnetic field B. Furthermore, the beam velocity (v_b) can be obtained from Equations (15) or (16). Together with the results of Section 3.2, we obtain a full diagnostic method of the flare energy-release site, including plasma density, temperature, magnetic field, and velocity and energy of the electron beams.

4 AN EXAMPLE

We take the microwave type III burst pairs at a frequency of 2.6–3.8 GHz observed by SBRS on 2006 December 13 as an example to test the above method in diagnosing the physical conditions of primary energy release. A type III burst pair is composed of a group of normal type III bursts (normal branch) with negative frequency drift rates and a group of RS type III bursts (RS branch) with positive frequency drift rates (Karlicky 2014; Tan et al. 2016).

Figure 2 presents spectrograms of three groups of microwave type III pairs in a long-duration powerful X3.4 flare. Table 1 lists their observed properties. Compared to the general microwave type III bursts, the microwave type III pair burst may provide much more information on the flare energy-release sites. The separation frequency (f_x) between the normal and RS branches can be used to replace the start frequency ($f_{\rm st}$) in Equation (6) to obtain the plasma density (n_x). By applying Equations (16) and (17) to the normal and RS branches, we can obtain an estimation of magnetic fields near the acceleration region.

The flare starts at 02:14 UT and peaks at 02:40 UT. The three microwave type III burst pairs occur at 02:45 UT, 03:29 UT and 03:45 UT, respectively, from several minutes to more than one hour after the flare maximum. All type III pairs show strong right-handed circular polarization overlaid on a long-duration broadband microwave type IV continuum in the post-flare phase. According to figure 13 of Tan et al. (2010), the distance between the two footpoints of the flaring loop is about $d \sim 2.0 \times 10^7$ m, assuming $t_n^{-1} \sim 0$ and $\cos\theta \sim 1$. Furthermore, the flaring loop is assumed to be a semicircle with $R_{\rm c} = \frac{1}{2}d \approx 1.0 \times 10^7$ m. Then, the diagnosed physical parameters of the acceleration region can be obtained which are listed in Table 1. We find the estimated magnetic fields near the acceleration region range from 53.6 ± 17.0 G to 87.4 ± 27.2 G. These values are a little less than the result estimated by microwave Zebra pattern structures in the same flare (90–200 G, Yan et al. 2007). As is well known, the Zebra pattern emissions are produced from the interior of the flare loop while the flare primary energy-release sites are above the flare loop. The energy of the electron beam associated with the RS type III branch is in the range of 42–64 keV, which is similar to that of the normal type III branches. This fact implies that accelerations are possibly identical for the upward and downward electron beams.

Table 1 also shows that the frequency drift rate of the normal type III branches is higher than that of RS branches. This fact can be explained as follows: from Equation (16) we have

$$\bar{D} \approx \frac{1}{2\mu_0 k_{\rm B}}\frac{B^2}{n_x T}\frac{v_b}{R_{\rm c}}. \quad (19)$$

It is well known that the electron beam from normal type III branches propagates upward in a relatively rarefied plasma (n_{xn}) while the electron beam from the RS branches propagates downward in a relatively denser plasma (n_{xr}) such that $n_{xn} < n_{xr}$. Equation (19) gives

Table 1 Estimation of the Physical Parameters in the Source Region of Type III Pairs Occurring in the Post-flare Phase of the X3.4 Flare on 2006 December 13

	Parameter	Type III pair A	Type III pair B	Type III pair C
Observation	Start time (UT)	02:45	03:29	03:45
	Lifetime: τ (s)	0.16	0.10	0.07
	Separation frequency: f_x (GHz)	2.92	3.42	2.90
	Frequency gap: δf (MHz)	50	260	10
	Normal III: $f_{\rm stn}$ (GHz)	2.895	3.290	2.895
	D_n (GHz s^{-1})	–14.5±0.6	–13.1±0.8	–10.5±1.2
	$\bar{D}_n$ (s^{-1})	–5.3±0.22	–4.4±0.26	–3.8±0.44
	RS III: $f_{\rm str}$ (GHz)	2.945	3.56	2.905
	D_r (GHz s^{-1})	8.6±0.8	5.6±0.6	9.7±0.8
	$\bar{D}_r$ (s^{-1})	2.6±0.24	1.5±0.16	3.2±0.26
Diagnostics	n_x (10^{17} m^{-3})	1.05	1.44	1.03
	T (10^7 K)	1.85	1.45	1.38
	n_n (10^{17} m^{-3})	1.035	1.336	1.035
	B_n (G)	87.4±27.2	80.2±26.5	70.4±26.4
	β_{pn}	0.87	1.05	1.00
	H_{nn} (km)	4.3×10^3	5.3×10^3	5.0×10^3
	v_n (c)	0.47	0.45	0.39
	E_n (keV)	64.1	58.0	42.3
	n_r (10^{17} m^{-3})	1.071	1.565	1.042
	B_r (G)	67.6±21.1	53.6±17.0	67.8±25.3
	β_{pr}	1.50	2.74	1.09
	H_{nr} (km)	7.5×10^3	1.4×10^4	5.5×10^3
	v_r (c)	0.47	0.46	0.39
	E_r (keV)	64.1	61.0	42.3
	$L_{\rm c}$ (km)	101	733	18

Notes: D is frequency drift rate, $\bar{D}$ is the relative frequency drift rate, and f_0 is the central frequency of the type III burst. f_x is the separation frequency between normal type III bursts and RS type III bursts. B is the magnetic field, and v and E are the velocity and energy of electron beams, respectively. $\beta_{\rm p}$ is the plasma beta value. The subscripts n and r indicate the normal and RS type III branches, respectively. $L_{\rm c}$ is the length of the acceleration region.

$\bar{D}_n > \bar{D}_r$, indicating that the normal branches drift faster than the RS branches.

Equation (19) shows that not only the plasma density ($n_{\rm e}$) affects the frequency drift rate, but also the magnetic field strength (B^2), plasma temperature (T), magnetic field configuration ($R_{\rm c}$) and the velocity of electron beams (v_b) dominate the value of drift rates. After determining these parameters, we can accurately explain the other observed properties of microwave type III burst pairs.

Additionally, we also calculate the plasma beta value ($\beta_{\rm p}$). The result is also listed in Table 1. Here, we find that the plasma beta is much greater than 1 which is just indicating that the flare primary energy-release region is a highly-dynamic area where the magnetized plasma is unstable which may generate plasma instability, trigger magnetic reconnection, accelerate particles, heat ambient plasmas, release magnetic energy and produce the flaring eruptions.

According to the PE mechanism, the frequency gap may imply a density difference between start sites of normal and RS type III bursts. With density scale length H_n, a spatial length can be derived

$$L_{\rm c} \approx H_{nn} \cdot \frac{\delta f}{2 f_{\rm stn}} + H_{nr} \cdot \frac{\delta f}{2 f_{\rm str}}. \quad (20)$$

$L_{\rm c}$ can be regarded as an estimation of the length of the acceleration regions. The electrons are accelerated in this region and acquire a relatively high energy, then trigger microwave type III bursts outside this region. The estimated length is about 18 – 733 km. It is possible that these results are the upper length limit of the acceleration region.

In the above estimation, we adopt the same value of $R_{\rm c}$ for both normal and RS type III branches. Actually, they are different from each other. However, Equation (2) indicates $B \propto R_{\rm c}^{1/2}$ and Equation (4) indicates $v_b \propto R_{\rm c} B^{-2}$. These facts show that the beam velocity (v_b) is independent of the magnetic field strength. So, the uncertainties in the magnetic field will not affect the estimation of velocity and energy in the electron beams.

5 CONCLUSIONS AND DISCUSSION

In summary, when considering the effect of the magnetic field on the plasma density and its distribution around the flare energy-release site, a relationship between the physical conditions and the observed parameters of microwave type III bursts can be established. With this relationship, we can directly diagnose the flare energy-release sites. The diagnostic procedure is as follows:

(1) Determine the temperature (T) at the time of a microwave type III burst from the observation of GOES SXR at wavelengths of 0.5–4 Å and 1–8 Å.
(2) Determine the plasma density ($n_{\rm st}$) using Equation (6) from the observed start frequency ($f_{\rm st}$) of a microwave type III burst or the separation frequency ($f_{\rm st}$) of microwave type III burst pairs.
(3) Estimate the magnetic field ($B_{\rm L}$ and B_H) by using Equations (17) and (18) from the observed relative frequency drift rate ($\bar{D}$), burst lifetime (τ) and the curvature radius of magnetic field lines ($R_{\rm c}$).
(4) Estimate the velocity and energy of the energetic electron beams using Equation (15) or (16) from the observed relative frequency drift rate ($\bar{D}$), the curvature radius of magnetic field lines ($R_{\rm c}$) and the above derived magnetic field strength (B).
(5) As for the microwave type III pairs, we may obtain an upper limit on the length of the acceleration region by using Equation (20) from the observed frequency gap (δf) between the normal and RS type III branches.

In the above diagnostic procedure, there is a key parameter $R_{\rm c}$. In the example given in Section 4, we obtained $R_{\rm c}$ by simply using the EUV imaging observation. Generally, such estimation is a bit more exact than deriving the plasma density scale length directly from the existing plasma density models. However, the above method is still a bit cursory. A more exact method to derive $R_{\rm c}$ depends on the radio spectral imaging observations at the corresponding frequencies, such as the Chinese Spectral Radioheliograph (CSRH, now renamed MUSER, Yan et al. 2009). By using such a new generation of telescopes, we may directly obtain the location and geometry of the source region, and derive a more exact value of the magnetic field scale length.

From the above diagnostics, we may acquire basic information on the study of the flare triggering mechanism and associated particle acceleration. However, the above method cannot be extended to type II bursts in meter or longer wavelengths because they propagate along open weak magnetic fields in the higher corona. Here, the magnetic field (B) becomes very weak and the curvature radius of magnetic field lines ($R_{\rm c}$) becomes very large, $\frac{B^2}{n_x \mu_0 R_{\rm c}} \ll m_0 g$, so Equation (13) degenerates to the barometric form $H_n \approx -\frac{k_{\rm B} T}{m_0 g}$. Then the above diagnostic method will depart from being a meaningful approximation.

Acknowledgements The authors thank Profs A. V. Stepanov, V. Melnikov and H. Hudson for their helpful suggestions and valuable discussions on this work. B. T. acknowledges support by the National Natural Science Foundation of China (Grant Nos. 11273030, 11221063, 11373039 and 11433006), MOST Grant (2014FY120300, CAS XDB09000000) and the National Major Scientific Equipment R&D Project (ZDYZ 2009-3). H. M. and M. K. acknowledge support by the Grant P209/12/00103 (GA CR) and the research project (RVO: 67985815) of the Astronomical Institute AS. This work is also supported by the Marie Curie PIRSES-GA-295272-RADIOSUN project.

References

Allen, C. W. 1947, MNRAS, 107, 426
Aschwanden, M. J., Benz, A. O., Dennis, B. R., & Schwartz, R. A. 1995, ApJ, 455, 347
Benz, A. O., Bernold, T. E. X., & Dennis, B. R. 1983, ApJ, 271, 355
Benz, A. O., Magun, A., Stehling, W., & Su, H. 1992, Sol. Phys., 141, 335
Cairns, I. H., & Melrose, D. B. 1985, J. Geophys. Res., 90, 6637
Dulk, G. A. 1985, ARA&A, 23, 169
Fu, Q., Qin, Z., Ji, H., & Pei, L. 1995, Sol. Phys., 160, 97
Fu, Q., Ji, H., Qin, Z., et al. 2004, Sol. Phys., 222, 167
Huang, J., Yan, Y.H., & Liu, Y.Y. 2007, Adv. Space Res., 39, 1439
Jiricka, K., Karlicky, M., Kepka, O., & Tlamicha, A. 1993, Sol. Phys., 147, 203
Karlický, M. 2014, RAA (Research in Astronomy and Astrophysics), 14, 753
Kliem, B., Karlický, M., & Benz, A. O. 2000, A&A, 360, 715
Lin, R. P., & Hudson, H. S. 1971, Sol. Phys., 17, 412
Lin, R. P., & Hudson, H. S. 1976, Sol. Phys., 50, 153
Lin, R. P., Potter, D. W., Gurnett, D. A., & Scarf, F. L. 1981, ApJ, 251, 364
Masuda, S., Kosugi, T., Hara, H., Tsuneta, S., & Ogawara, Y. 1994, Nature, 371, 495
Melrose, D. B., & Dulk, G. A. 1982, ApJ, 259, 844
Newkirk, Jr., G. 1967, ARA&A, 5, 213
Priest, E. 2014, Magnetohydrodynamics of the Sun (Cambridge, UK: Cambridge Univ. Press)
Reid, H. A. S., & Ratcliffe, H. 2014, RAA (Research in Astronomy and Astrophysics), 14, 773
Robinson, P. A., & Benz, A. O. 2000, Sol. Phys., 194, 345
Stahli, M., & Benz, A. O. 1987, A&A, 175, 271
Tan, B., Yan, Y., Zhang, Y., et al. 2009, Science in China: Physics, Mechanics and Astronomy, 52, 1765
Tan, B., Zhang, Y., Tan, C., & Liu, Y. 2010, ApJ, 723, 25
Tan, B. L., Mészárosová, H., Karlický, M., Huang, G. L., & Tan, C. M. 2016, ApJ, 819, 42
Tang, J. F., Wu, D. J., & Yan, Y. H. 2012, ApJ, 745, 134
Thomas, R. J., Crannell, C. J., & Starr, R. 1985, Sol. Phys., 95, 323
Yan, Y. H., Tan, C.M., & Xu, L., et al. 2002, ScChA, 45, 89
Yan, Y., Huang, J., Chen, B., & Sakurai, T. 2007, PASJ, 59, 815
Yan, Y., Zhang, J., Wang, W., et al. 2009, Earth Moon and Planets, 104, 97
Zharkova, V. V., Arzner, K., Benz, A. O., et al. 2011, Space Sci. Rev., 159, 357
Zheleznyakov, V. V., & Zlotnik, E. Y. 1975, Sol. Phys., 44, 461